Title
Nonlocal Modeling and Swarm-Based Design of Heat Sinks

Journal
Journal of Heat Transfer, 136(1)

ISSN
0022-1481

Authors
Geb, David
Catton, Ivan

Publication Date
2014

DOI
10.1115/1.4025300

Peer reviewed

Nonlocal Modeling and Swarm-Based Design of Heat Sinks

David Geb* **and Ivan Catton**
University of California, Los Angeles
School of Engineering and Applied Science
Department of Mechanical and Aerospace Engineering
Morrin-Gier-Martinelli Heat Transfer Memorial Laboratory
48-121 Engineering IV, 420 Westwood Plaza, Los Angeles, CA, 90095-1597

ABSTRACT

Cooling electronic chips to satisfy the ever-increasing heat transfer demands of the electronics industry is a perpetual challenge. One approach to addressing this is through improving the heat rejection ability of air-cooled heat sinks, and nonlocal thermal-fluid-solid modeling based on Volume Averaging Thoery (VAT) has allowed for significant strides in this effort. A number of optimization methods for heat sink designers who model heat sinks with VAT can be envisioned due to VAT's singular ability to rapidly provide solutions, when compared to Direct Numerical Simulation (DNS) and Computational Fluid Dynamics (CFD) approaches. The Particle Swarm Optimization (PSO) method appears to be an attractive multi-parameter heat transfer device optimization tool, however it has received very little attention in this field compared to its older population-based optimizer cousin, the Genetic Algorithm (GA). The PSO method is employed here to optimize smooth and scale-roughened straight-fin heat sinks modeled with VAT by minimizing heat sink thermal resistance for a specified pumping power. Optimal designs are obtained with the PSO method for both types of heat sinks, the performances of the heat sink types are compared, and the performance of the PSO method is discussed with reference to the GA method. This study demonstrates the effectiveness of combining a VAT-based nonlocal thermal-fluid-solid model with population-based optimization methods, such as PSO, to design heat sinks for electronics cooling applications.

* Corresponding Author (Email: dvdgb15@ucla.edu, Phone: 805-765-7669)

Key Words: Volume Averaging Theory, Particle Swarm Optimization, Heat Sink, Optimization, Genetic Algorithm, Electronics Cooling, Heat Transfer Augmentation

INTRODUCTION

Past studies have considered different methods for the optimization of heat sink designs. Much emphasis, in particular, has been placed on optimization with Genetic Algorithms (GAs). While early work on GAs for general optimization problems was performed in the 1970s and 1980s by Holland [1], Goldberg [2], and others, GAs for electronics cooling applications didn't begin to receive attention until the work of Queipo, Devarakonda, and Humphrey [3] in the mid-1990s. Since then a number of heat sink optimization studies using GAs have been reported, with various modeling approaches. Some investigators have used algebraic correlations of the heat sink performance, e.g. thermal resistance or entropy generation, as the model on which the GA operates [4-6]. Others have interfaced Direct Numerical Simulations (DNS) and Computational Fluid Dynamics (CFD) packages with GAs to perform optimization [3, 7, 8]. Further, others have coupled porous media models with GAs to optimize heat sink designs [9-11].

Less emphasis, however, has been placed on heat sink design with Particle Swarm Optimization (PSO). PSO was developed in the 1990s by Kennedy, Eberhart, and their students [12-19], and began to receive attention for electronics cooling applications in the early 2000s. In particular, CFD heat sink simulations have been interfaced with the PSO method to optimize heat sink designs in several recent studies [20-22].

The heat sink modeling methods thus far employed with the PSO and GA optimization tools suffer from some undesirable characteristics. Although those modeling methods using algebraic performance correlations yield fast performance evaluations, allowing the PSO and GA to

thoroughly explore the design/solution space, these methods' applicability are confined to the certain conditions from which they were derived and do not afford the flexibility that full simulations provide. Full simulation modeling methods using DNS and CFD can provide detailed solutions of the flow and temperature fields for different flow regimes and arbitrary channel morphologies, and at first seem ideal as a model on which to perform optimization. However, DNS and CFD solutions used for optimization typically either don't include the conjugate heat transfer effects, i.e. the solid side, or carry a large computational burden when attaining the many solutions necessary that cripples the PSO and GA's search abilities. Some porous media models show promise for certain applications, however, the models typically employed are empirically-based, often don't include conjugate effects, and don't incorporate clearly defined transport coefficients. The VAT-based hierarchical modeling methodology presented here to overcome these undesirable characteristics performs full thermal-fluid-solid simulations that account for the flow regime and arbitrary channel morphologies, includes full conjugate heat transfer effects, is general and rigorously derived from fundamental equations, incorporates clearly defined transport coefficient expressions, and provides fast computational times that allow PSO and GA optimizations to be easily realized with even modest computing hardware.

The VAT-based fluid mechanics and thermal energy equations modeling hierarchical momentum and heat transport within a heterogeneous porous medium, like a heat sink channel, are derived from the Navier-Stokes and solid and fluid thermal energy equations, and are the basis for studying fluid flow and thermal phenomena in porous media [23]. Work on VAT began with contributions by Anderson and Jackson [24], Slattery [25], Marle [26], Whitaker [27], and Zolotarev and Radushkevich [28], and continued with contributions by Slattery[29], Kaviany

[30], Gray et al. [31], Whitaker [32, 33], Kheifets and Neimark [34], Dullien, [35] and Adler [36] among others. Travkin, Catton and coauthors [37-41] extended its application to nonlinear and turbulent transport in porous media and recently Nakayama and coauthors [42-45] have contributed to continuing VAT's development. Due to the averaging process, the VAT-based governing equations yield additional integral and differential terms when compared to the homogenized or classical continuum mechanics equations. Travkin and Catton [46] devoted some effort to relate these terms to the local transport coefficients. Once these additional terms are closed, the resulting equation set is relatively simple, the device morphology is directly incorporated, and its solution can be quickly obtained using basic numerical methods, thus opening the door to population-based optimization methods, such as PSO.

The PSO method, as employed here, was discovered by Eberhart and Kennedy [12] while performing simulations of a simple social model, and since then it has proven itself to be both fast and robust in solving a wide range of nonlinear, non-differentiable, multi-modal optimization problems. As Eberhart and Kennedy describe, it is a simple concept, can be implemented in just a few lines of computer code, requires only primitive mathematical operators, and is computationally inexpensive in terms of both memory requirements and speed. PSO is part of a long line of biologically-inspired algorithms and can be thought to lie somewhere in between Genetic Algorithms (GAs) and Artificial Neural Networks (ANNs). While evolution by natural selection (i.e. GAs) may take eons and neural processing (i.e. ANNs) may take milliseconds, social optimization (i.e. PSOs) occurs in the time frame of ordinary experience. In PSO, they explain, individuals improve through *cooperation* and *competition* among themselves in the same way individuals in a flock, school, herd, or swarm profit from the discoveries and experiences of other members of the group during their search for desirable resources that are

unpredictably distributed. It is based on the premise that social sharing of information offers an evolutionary advantage. Additionally, they observed that in a similar fashion to the way birds and fish move through three-dimensional space to seek food and mates, avoid predators, and optimize their environment, humans adjust their beliefs and attitudes to conform with their peers and societal norms in an abstract multi-dimensional space. Therefore PSO also has roots in human learning patterns.

In this study, the PSO method is implemented for optimizing heat sinks modeled with VAT. Such a modeling methodology was recently incorporated with a GA to optimize a two-fluid stream heat exchanger [47]. Here, both smooth surface and scale-roughened surface straight-fin heat sinks with tapered fins are considered, see Figure 1. The results from the PSO method are compared to and verified against results from a GA. The performance of these two types of heat sinks and the effectiveness of the nonlocal modeling coupled with a swarm-based design strategy are then discussed.

TRANSPORT MODEL

The VAT-based upper-scale transport model employed here was presented in [46] and the references therein, and is derived from the lower-scale Navier-Stokes and thermal energy equations in the fluid and solid phases. The steady-state, incompressible, VAT-based governing equations accounting for turbulent transport in porous media follow. The continuity equation is trivial. The one-dimensional momentum equation is written as

$$\frac{\partial}{\partial z}\left[\left\langle m(z)\right\rangle\left(\tilde{\nu}_T+\nu\right)\frac{\partial\tilde{\bar{u}}(z)}{\partial z}\right]+\frac{\partial}{\partial z}\left(\left\langle\tilde{\nu}_T\frac{\partial\tilde{\bar{u}}}{\partial z}\right\rangle_f\right)+\frac{\partial}{\partial z}\left(\left\langle-\hat{\bar{u}}\hat{\bar{w}}\right\rangle_f\right)$$
$$+\frac{1}{\Delta\Omega}\int_{\partial S_{wT}}\nu_T\frac{\partial\bar{u}}{\partial x_i}\cdot d\vec{s}+\frac{1}{\Delta\Omega}\int_{\partial S_{wL}}\nu\frac{\partial\bar{u}}{\partial x_i}\cdot d\vec{s}-\frac{1}{\rho_f\Delta\Omega}\int_{\partial S_w}\bar{p}\cdot d\vec{s}=\frac{1}{\rho_f}\frac{\partial\langle\bar{p}\rangle_f}{\partial x} \quad (1)$$

The two-dimensional thermal energy equation in the fluid phase is written as

$$\rho_f c_{pf} \langle m \rangle \tilde{\bar{u}}(z) \frac{\partial \tilde{\bar{T}}_f(x,z)}{\partial x} = \langle m \rangle \frac{\partial}{\partial x}\left[\left(\tilde{k}_T + k_f \right) \frac{\partial \tilde{\bar{T}}_f(x,z)}{\partial x} \right] + \langle m \rangle \frac{\partial}{\partial z}\left[\left(\tilde{k}_T + k_f \right) \frac{\partial \tilde{\bar{T}}_f(x,z)}{\partial z} \right] + \frac{1}{\Delta\Omega} \int_{\partial S_{wL}} k_f \frac{\partial \bar{T}_f}{\partial x_i} \cdot d\vec{s} + \frac{1}{\Delta\Omega} \int_{\partial S_{wT}} k_T \frac{\partial \bar{T}_f}{\partial x_i} \cdot d\vec{s} \quad (2)$$

The two-dimensional thermal energy equation in the solid phase is written as

$$\frac{\partial}{\partial x}\left[\left(1 - \langle m \rangle \right) k_s(x,z) \frac{\partial \tilde{T}_s(x,z)}{\partial x} \right] + \frac{\partial}{\partial z}\left[\left(1 - \langle m \rangle \right) k_s(x,z) \frac{\partial \tilde{T}_s(x,z)}{\partial z} \right] + \frac{1}{\Delta\Omega} \int_{\partial S_w} k_s \frac{\partial T_s}{\partial x_i} \cdot d\vec{s}_1 = 0 . \quad (3)$$

The mean eddy viscosity is given by

$$\tilde{\nu}_T = C_\mu l(z) \sqrt{b} , \quad (4)$$

where $l(z)$ is the turbulent scale function defined by the assumed porous medium structure. The equation for the mean turbulent fluctuation energy $b(z)$ is written as

$$\tilde{\nu}_T \left(\frac{\partial \tilde{\bar{u}}}{\partial z} \right)^2 + \frac{d}{dz}\left[\left(\frac{\tilde{\nu}_T}{\sigma_b} + \nu \right) \frac{db}{dz} \right] + c_d S_w \tilde{\bar{u}}^3 + 2\nu \left(\frac{db^{1/2}}{dz} \right)^2 - \frac{g}{T\sigma_b} \left(\tilde{\nu}_T \frac{d\tilde{\bar{T}}}{dz} \right) = C_D C_\mu \frac{b^2}{\tilde{\nu}_T} . \quad (5)$$

The averaging procedure used to obtain the upper-scale governing equations yields additional integral and differential terms, embodying the closure problem, which must be dealt with.

Travkin and Catton [46] devoted some effort to relate these additional terms to the local drag and heat transfer coefficients. The local drag coefficient is in general expressed as

$$c_d = 2\frac{\int_{\partial S_w} \bar{p}\cdot d\vec{s}}{\rho_f \tilde{\bar{u}}^2 A_{wp}}\cdot\frac{S_{wp}}{S_w} + 2\frac{\int_{\partial S_w} \tau_{wL}\cdot d\vec{s}}{\rho_f \tilde{\bar{u}}^2 A_w} + 2\frac{\int_{\partial S_w} \tau_{wT}\cdot d\vec{s}}{\rho_f \tilde{\bar{u}}^2 A_w} - \frac{\frac{\partial}{\partial x_j}\left\langle \hat{\bar{u}}_i \hat{\bar{u}}_j \right\rangle_f}{\frac{1}{2}\rho \tilde{\bar{u}}^2} + \frac{\frac{\partial}{\partial x_j}\left(\left\langle \tilde{\nu}_T \frac{\partial \tilde{\bar{u}}_i}{\partial x_j} \right\rangle_f \right)}{\frac{1}{2}\rho \tilde{\bar{u}}^2}, \tag{6}$$

and the local heat transfer coefficient is in general expressed as

$$h = \frac{\frac{1}{\Delta\Omega}\int_{\partial S_w} \left(k_f + k_T\right)\nabla \bar{T}_f \cdot d\vec{s} - \rho_f c_{p_f} \nabla\cdot\left(\langle m \rangle \left\{ -\hat{\bar{u}}\hat{\bar{T}}_f \right\}_f \right) + \nabla\cdot\left(\frac{k_f}{\Delta\Omega}\int_{\partial S_w} \bar{T}_f d\vec{s} \right)}{S_w\left(\tilde{T}_s - \tilde{\bar{T}}_f\right)}. \tag{7}$$

Zhou et al. [48] present correlations for c_d and h, developed from lower-scale CFD simulations, that close the VAT-based governing equations for the smooth and scale-roughened surface straight-fin heat sinks considered here. Having found closure for the surfaces under consideration, the governing equations become simple and solutions may be readily obtained numerically, opening the door to population-based optimization efforts.

COMPUTATIONAL METHODS AND SOLUTION PROCEDURE

The VAT-based momentum, turbulent kinetic energy, and thermal energy equations are solved numerically with the finite difference method over the two-dimensional x-z plane. In particular, statements for one-dimensional fully developed turbulent flow and two-dimensional, two-temperature heat transfer in a porous layer and heat transfer in a base plate are used. Uniform gridding is employed in the base plate, when it is considered, and over most of the

channel, however a higher density grid in the flow (x) direction is implemented near the channel inlet and outlet regions. A flow chart of the solution algorithm is illustrated in Figure 2.

After the problem is formulated and the variables are initialized, the velocity distribution for turbulent channel flow in porous media is simulated for incompressible, constant property flow, i.e. it is uncoupled from the thermal routine. Subsequently, the two-dimensional, two-temperature statements modeling the turbulent heat transfer in the fluid phase and the conjugated heat transfer in the solid phase are solved using the velocity field and turbulence parameters as input. To resolve the temperature fields there are several iterative loops, as indicated in Figure 2. When the base plate is considered, an inner loop converges the fluid and solid channel temperatures using a form of ADI. Another inner loop converges the base temperature separately from the channel temperatures, given an interface temperature between the channel and base and a bottom base temperature or heat flux. An outer loop then matches the interface heat flux and temperature between the base and channel by varying the interface temperature. If the base plate is not considered then a simpler situation arises, and a single loop simply converges the fluid and solid channel temperatures. When the VAT-based solution routine exits, the fully-developed velocity field and two-dimensional temperature fields are obtained, along with other relevant calculated quantities, e.g. the thermal resistance.

During the optimization runs in this study the base plate is neglected, to provide quicker solution times, and a constant temperature boundary condition is imposed on the bottom of the channel. The results of the optimization are then verified by including the base plate and solving for a uniform heat flux boundary condition on the bottom of the base plate. This method stems from the assumption that the performance of a heat sink with no base plate and a constant

temperature boundary condition is related to the performance of a heat sink with a thin base plate and a uniform heat flux boundary condition.

In this study the fluid is air and the heat sink is aluminum for all cases and several geometric parameters of the heat sink are kept fixed, as indicated in Figure 1. Additionally, appropriate flow and thermal boundary conditions are kept fixed throughout the study. A fixed pumping power of 30W, and no-slip boundary conditions at the bottom and top of the channel fully specify the flow field through the given channel geometry. To specify the thermal fields in both the solid and fluid phases, a uniform inlet air temperature of 30°C is implemented, along with an adiabatic condition at the top of the channel, and one of two lower thermal boundary conditions. The lower thermal boundary condition is a 90°C isothermal one at the bottom of the channel during the optimization, where the base plate is neglected. After the optimization, the designs are evaluated with a uniformly distributed 1kW heat source at the bottom of the baseplate as the lower thermal boundary condition.

PARTICLE SWARM OPTIMIZATION

The ability to quickly obtain solutions provided by the VAT-based modeling and solution routine outlined above allows for population-based optimization to proceed. In the present study the multi-parameter, constrained optimization problem is formulated as follows. The heat sink thermal resistance, $R_{th}(X)$, is to be minimized over the bounded search domain

$$X \equiv \left(\delta_{\text{base}}, \delta_{\text{top}}, H_f, S_y\right), \tag{8}$$

where the parameters are bounded between minimum and maximum values $X_{\min}$ and $X_{\max}$ respectively, as shown in Table 1. Tapering of the fins is allowed during the search and the fin

thickness varies linearly with respect to the z-coordinate. Optimization should yield X^* and $R_{th}^* = R_{th}\left(X^*\right)$, the optimal solution and its corresponding thermal resistance, respectively.

Each individual, i.e. heat sink design, in the PSO is treated as a particle, defined by its position, that flies through $D = 4$-dimensional hyperspace. In general, the ith particle is represented as $X_I = \left(x_{i1}, x_{i2}, ..., x_{iD}\right)$, its best previous position as $P_I = \left(p_{i1}, p_{i2}, ..., p_{iD}\right)$, and its velocity as $V_I = \left(v_{i1}, v_{i2}, ..., v_{iD}\right)$. The index of the best particle in the neighborhood is n. Each particle adjusts it flight according to

$$v_{id} = w \times v_{id} + c_1 \times rand(\,) \times \left(p_{id} - x_{id}\right) + c_2 \times Rand(\,) \times \left(p_{nd} - x_{id}\right), \tag{9}$$

$$x_{id} = x_{id} + v_{id}, \tag{10}$$

where c_1 and c_2 are two "learning factors", $rand(\,)$ and $Rand(\,)$ are two independently generated random numbers in the range $[0,1]$, and w is the "inertia weight" [14]. Equation (9) calculates the particle's new velocity according to its weighted previous velocity and stochastic functions of the distance of its current position from its own best position and that of the group. The particles then "fly" toward a new position according to Equation (10).

The first term on the right side of Equation (9) is the particle's previous velocity multiplied by an inertia weight. The inertia weight is employed to control the impact of the previous history of velocities on the current velocity, and influences the tradeoff between global and local exploration. A larger inertia weight facilitates global exploration while a smaller inertia weight facilitates local fine-tuning. The second term on the right side of Equation (9) is the "cognition" part, representing the private thinking of the individual particle, and contributes to a stochastic

change in velocity [49]. Conceptually, p_{id} resembles autobiographical memory, as each individual remembers its own experience, and the velocity adjustment associated with this term can be viewed as "nostalgia" in that the individual tends to return to the place that most satisfied it in the past. The third term on the right side of Equation (9) is the "social" part, representing collaboration among the particles, and contributes to a stochastic change in velocity. Conceptually, p_{nd} resembles publicized knowledge, or a group norm or standard, which individuals seek to attain.

To implement the PSO, the particle population is initially randomized, as in the GA, and subsequently searches for optima by updating iteratively through time. In every iteration, each particle is updated by its attraction to its own best position p_{id}, and that of its neighbors p_{nd}, through Equations (9) and (10). When a given criterion is satisfied, the iteration exits with what is taken to be the optimal solution. A flow chart of the general PSO algorithm used here is shown in Figure 3, [50]. The algorithm employed here randomly finds N_S neighbors for each particle at each iteration, uses a well-tested random number generator, exits after a fixed number of iterations N_G, and implements the settings tabulated in Table 2.

RESULTS AND DISCUSSION

Employing the VAT-based modeling and solution routine coupled with the PSO technique, smooth and scale-roughened straight-fin heat sinks are optimized by minimizing their thermal resistance while maintaining a constant pumping power. Boundary conditions and certain parameters are fixed as detailed above and other parameters are variable with search ranges tabulated in Table 1. Results from the optimization of smooth surface and then scale-roughened surface fins are first considered in this section, followed by a discussion on the evolution of the

nonlocal flow and temperature fields and an evaluation of the performance of the PSO method in relation to the GA method.

Smooth Surface Fins

The first case considered is for a simple smooth surface straight-fin heat sink, Figure 1a. The PSO evolves the optimal design over iterations so that the heat sink thermal resistance favorably evolves. Ten independent PSO trials are run and the evolution of the optimal thermal resistance for the ten individual trials (thin grey lines) along with the average of the ten trials (thick black line) are plotted in Figure 4a. The inset of Figure 4a shows closely the first few iterations before which all ten trials converge to the optimum. By the 16th iteration, all ten independent trials agree on the same value for the optimal R_{th}, i.e. 0.079 °C/W without the base plate. Alternatively, from the perspective of the design space, the ten independent PSO trials evolve scaled values of H_f, S_y, δ_{base}, and δ_{top} as illustrated in Figure 5a. Here the search ranges of the four design parameters are scaled between 0 and 1, where 0 is the minimum value and 1 is the maximum, see Table 1. That is,

$$\bar{X} = \frac{X - X_{\min}}{X_{\max} - X_{\min}}, \tag{11}$$

where $\bar{X}$ is the scaled design space vector. While the color-coded thin lines in Figure 5a indicate the evolution of the optimal parameters for the ten independent trials, the color-coded thick lines indicate the average over the ten trials. Evident from Figure 5a is that, in addition to all ten trials converging to a single optimal value R_{th}^*, all ten trials also converge to a single optimal solution in the design space, X^*, for the ten individual PSO runs.

As a comparison to the PSO, a GA is run for the same problem. A basic single-objective GA is employed that is inspired primarily by the work of Holland [51] and Goldberg [2]. The particular details of the GA being used here were presented in more detail in [47], where it was applied to a two-stream heat exchanger with ten design parameters. The GA operation settings used in the present study are given in Table 3. The GA similarly evolves the optimal design over generations so that the heat sink thermal resistance favorably evolves, Figure 4b, although the GA operates based on genetic rather than social mechanisms. It is apparent from Figure 4b, and emphasized in its inset, that convergence is not realized as quickly as for the PSO method. Again, ten independent trials are run for the GA optimization. The optimal thermal resistance for smooth surface straight-fin heat sinks found by the GA for all ten trials is also 0.079 °C/W, and by the 247th generation, all ten individual GA trials have converged to this value. Again, from the perspective of the design space, the GA evolves scaled values of H_f, S_y, δ_{base}, and δ_{top} as shown in Figure 5b. Again, it is evident from this figure that all ten trials have converged to an optimal solution in the design space, X^*, for the ten individual GA runs.

Table 4 tabulates the characteristics of the optimized smooth surface straight-fin heat sinks produced by both the PSO and the GA methods. Included in this table is the thermal resistance found by the PSO and GA without the base plate and an isothermal lower boundary condition, and that evaluated with the base plate and a uniform heat flux lower boundary condition. Evident is the 9% increase in thermal resistance resulting from considering the base plate. From Table 4, and from careful inspection of Figure 5, one can observe that while the optimal thermal resistance value R_{th}^* and most of the optimal design parameter values X^* obtained by both the PSO and GA agree, the optimal value of H_f found by the GA is slightly smaller than that obtained by the PSO. In other words, the GA's solution sacrifices side-fin surface area and fin

conduction in a very small layer at the top of the channel for both a slight flow bypass and exposure of the top surface of the fins. Although it results in a new design from that produced by the PSO its performance in terms of R_{th} is equivalent.

Scale-Roughened Surface Fins

The previous section considered smooth surface fins. It has previously been shown that augmenting the fin surface with scales enhances the heat transfer without a significant increase in pressure drop [52]. Moreover, recent advances in three-dimensional metal printing techniques [53] make such surfaces readily attainable. A small or moderate increase in the heat transfer coefficient can more than offset even a large friction factor increase because flow velocity can then be decreased and friction power varies with as much as the cube of velocity [54]. The second optimization study uses the surface scales investigated by Chang et al. [52] and more broadly correlated by Zhou et al. [48], and employs a fixed scale diameter D of 1.00mm and a fixed scale height e of 0.10mm. The parameters that are varied and their ranges are the same as for the smooth surface case, see Table 1. That is, everything is the same as before except now the fin surfaces are augmented with a high performance surface, Figure 1b.

The optimized configurations of the scale-roughened straight-fin heat sink obtained with the PSO and GA both give a thermal resistance of 0.056 °C/W when the base plate is neglected, which translates to 0.058 °C/W when the base plate is incorporated, a 4% increase. The geometric parameters are evolved again in ten independent trials by the PSO and GA and the corresponding heat sink thermal resistance evolves as shown in Figure 6. The ten individual PSO trials all converge to an optimum value of R_{th} within 13 iterations while the ten individual GA trials all converge within 187 generations. From the perspective of the design space, the PSO and GA evolve scaled values of H_f, S_y, δ_{base}, and δ_{top} as shown in Figure 7. Again, as for

the case of the smooth surface straight-fin heat sink, in addition to all ten trials converging to an optimal value for R_{th}, all ten trials have also converged to a single optimal solution in the design space for both the PSO and GA methods. The primary difference in the optimal designs between the two types of heat sinks is that for the scale-roughened surface straight-fin heat sink the fins have opened up slightly compared to the smooth surface heat sink.

The characteristics of the optimized heat sink with surface scales found by both the PSO and the GA are compared in Table 5. Again the GA favored a very slight by-pass flow as for the smooth surface case. By comparing Table 4 and Table 5 it is evident that the optimal scale-roughened straight-fin heat sink outperforms the optimal smooth surface heat sink in terms of thermal resistance by 33%. The higher performance of the scale-roughened surface compared to the smooth surface can be attributed to the frequent boundary layer interruption caused by the scales that precludes thickening of the boundary layer.

Evolution of the Nonlocal Velocity and Temperature Fields

What distinguishes the present study from those in the past, as was discussed in the Introduction, is that the population-based optimization methods employed here operate on full nonlocal simulations of turbulent flow and heat transfer within and between the fluid and solid phases of the heterogeneous and hierarchical medium. The upper-scale governing field equations are rigorously derived from fundamental lower-scale equations, and full conjugate effects are included. The local transport coefficients, such as the internal heat transfer coefficient that connects the fluid and solid phase thermal energy equations together, are derived from lower scale equations, as presented in Equations (6) and (7). It is therefore relevant to observe the evolution of the nonlocal flow field and temperature fields in both the fluid and solid phases during a PSO trial.

The velocity and fluid and solid temperature fields evolve during a single trial of the PSO of a scale-roughened straight-fin heat sink as shown in Figure 8a-c. Figure 8a illustrates the best solution after the first iteration, Figure 8b shows the best solution after the 4^{th} iteration, and Figure 8c does so for the converged solution, i.e. after the 13^{th} iteration. Figure 8d displays the converged solution of the PSO for the *smooth* surface straight-fin heat sink as a comparison. The temperature fields in the figure are scaled between 30°C and 120°C and the x and z direction coordinates indicate the position in the temperature contours in mm. The velocity magnitude is indicated in m/s by the x coordinate (i.e. $x-30$) as a function of the z direction coordinate which is again indicated in mm. Note in the figure that the solid phase temperature contours include the base plate while the fluid phase temperature contours do not as the fluid phase is only defined in the channel. The details of the heat sink designs considered in Figure 8 are tabulated in Table 6 for easy reference.

Evident from Figure 8a is that the solution after the first iteration, i.e. the best among N_P randomly selected designs, is far from favorable. Table 6 indicates that the fins reach about 70% of the channel height, and that they are relatively thick from the base to the top. It may be observed from the velocity profile that a significant bypass flow results from this design. Moreover, it may be observed that the fluid temperature $\tilde{\tilde{T}}_f$ becomes very hot around the fins while the flow above the fins stays very cold and is not serving to remove heat. Looking at the solid temperature field $\tilde{T}_s$ one can see that very high temperatures persist. Assuming that temperatures in the heat sink greater than 90°C are unacceptable for the electronics being cooled, and indicating the 90°C contour with a dashed white line, it is evident that this design is far from acceptable, with the maximum temperature incurred being $\tilde{T}_{s,\max} = 111.09°\text{C}$ (and occurring in

the bottom of the base plate at the outlet). As a side note, one may observe that $\tilde{T}_s$ is defined throughout the channel in Figure 8a even where the fins do not reach. By referring back to Equation (3) this is reconciled by observing the influence of the local morphology functions, i.e. $\langle m \rangle$ and S_w, which above the fins are unity and null respectively.

It is evident from Figure 8b that the solution resulting from the 4th iteration is noticeably improved from that previously considered. In this design the fins rise to the full channel height, however the base of the fins is unnecessarily thick. The velocity profile, now without a significant bypass flow, indicates that slightly higher flow velocities occur higher in the channel due to the thinning of the fins and opening of the cross flow area. The fluid temperature does not incur very high local temperatures as was the case for the previous design. Moreover, the solid temperature field is noticeably cooler than for the previous design, with the location of the 90°C contour line indicating that the design is approaching an acceptable one. The maximum temperature incurred for this design is $\tilde{T}_{s,\max} = 98.37°\mathrm{C}$.

Figure 8c presents the solution for the optimized design. In this design the fin height was maximized, the fin thickness from the base to the top was minimized, and the fin pitch was balanced. The velocity profile is symmetric about the channel centerline and the fluid temperature stays cool throughout the domain, allowing the solid phase to remain cool while still providing sufficient heat flow. From the absence of the 90°C contour line in Figure 8c, it is evident that the optimal design stays sufficiently cool. The maximum temperature incurred for the optimal design, in fact, is $\tilde{T}_{s,\max} = 87.73°\mathrm{C}$.

As a comparison to the optimized scale-roughened straight-fin heat sink solution depicted in Figure 8c, Figure 8d provides the solution to the optimized *smooth* straight-fin heat sink. The only differences between the two designs are the fin surface augmentation and the resulting fin

pitch. Evident from the figure is that a similar symmetric velocity profile results, with slightly lower magnitudes as a result of the smaller fin pitch, i.e. higher number of fins on the heat sink. The fluid temperature field appears somewhat similar to that found for Figure 8b in terms of magnitude and distribution. However, without the surface-scale augmentation, the temperature difference between the solid and fluid must be higher to provide the same heat removal ability, and in this case the entire solid temperature domain is greater than 90°C, with the maximum temperature incurred being $\tilde{T}_{s,\max} = 116.19°\mathrm{C}$. Together Figure 8c and Figure 8d illustrate the benefits of augmenting the fin surface with scales.

Performance of the Particle Swarm Optimization Method

Each optimization method, i.e. PSO and GA, delivers the same heat sink performance R_{th}^* for both heat sink types, i.e. smooth and scale-roughened fin surfaces. The time each takes to do so differs, however. In this study the PSO finds the optimum significantly quicker than the GA does, $\sim 10^{-1}$ seconds quicker in fact. The performance, in particular the convergence speed, of both population-based optimization methods depends on the methods' settings for a particular problem. Since no effort was made to customize these settings in this study (rather, typically used or suggested values were employed for the settings, see Table 2 and Table 3) conclusions about which method is faster for this particular problem cannot be determined. A future study could explore this by first optimizing each method's settings for the problem and then comparing the two methods' convergence speed. Fortunately, the VAT-based nonlocal modeling method provides solutions very quickly, compared to DNS and CFD, affording designers the luxury of proceeding without fine-tuning the optimization methods' operation parameters.

As was noted above, the GA located optimal designs for both heat sink types with a very slight flow bypass arrangement that exposed the top surface of the fins. Although the optimal

heat sink thermal resistances found by the GA were equivalent to those found by the PSO, the solutions – or designs – were distinct. The PSO's superior convergence speed for the problem and settings considered here is at least partly due to its inclination to explore the solution domain's boundaries relatively early in its search. Since several of the optimal designs' parameters lay on the boundary, the PSO settled on these without much exploration of the rest of the domain. The GA on the other hand operated more methodically and slowly, more thoroughly traversing the search domain in its search for the optimal design. Although the GA ultimately selected δ_{base} and δ_{top} values at the edge of the domain, it settled on a value of H_f just short of the domain's edge, and found no motivation to move this value to the edge of the domain, where the PSO had settled.

Over the course of ten trials, on a 2.20 GHz Intel Core i7-2720QM CPU with 16.0 GB of RAM and for the settings listed in Table 2, the compiled Fortran PSO code runs for an average of 6 minutes and 15.2 seconds with N_G changed from 150 to 16 for the smooth surface heat sink and 5 minutes and 37.5 seconds with N_G changed to 13 for the scale-roughened heat sink. As a comparison, over the course of ten trials for the settings tabulated in Table 3 the compiled Fortran GA code runs for an average of 1 hour, 7 minutes and 27.5 seconds, with N_G changed from 300 to 247 for the smooth surface heat sink and 1 hour, 2 minutes and 23.3 seconds with N_G changed to 187 for the scale-roughened heat sink. It is evident that either the PSO or the GA methods with standard settings provide optimal designs in a reasonable amount of time even on modest equipment due to their reliance upon the nonlocal physical modeling provided by VAT. As a comparison, running even a single heat sink simulation, never mind any kind of optimization endeavor, with CFD on the same equipment would cost hours.

CONCLUSIONS

In this paper a VAT-based nonlocal model of transport phenomena in a porous channel used to simulate flow and heat transfer in a heat sink for cooling electronic devices was the basis for a population-based optimization study. The VAT-based simulation routine was coupled with a single objective PSO design tool in order to perform heat sink optimizations. Results from the PSO method were compared to and verified against those from the GA method. Two different types of straight-fin heat sinks were considered, i.e. one type with smooth surface fins and another with scale-roughened surface fins. The performance of the two types of heat sinks was discussed as was the performance of the two methods of optimization.

It was observed that both optimization methods deliver equivalent optimized heat sink designs in terms of heat sink thermal resistance, however judgment on which method performs better for this particular problem was reserved. It was found that the nonlocal modeling based on VAT allows the PSO and GA methods to obtain optimal designs within several minutes and around an hour respectively on a modest lap top without customizing the optimization methods' settings, providing more freedom in selecting computational design tools for heat sink designers. Moreover, it was observed that augmenting the fins with scales improves the heat sink performance in terms of thermal resistance by 33%. The paper demonstrates that the nonlocal thermo-fluid-solid modeling provided by VAT opens the door to easily-implemented and thorough population-based optimization studies of heat sinks.

ACKNOWLEDGMENTS

The support of the DARPA MACE program Grant No. W31P4Q-09-1-0005 is gratefully acknowledged. The views, opinions, and/or findings contained in this article are those of the authors and should not be interpreted as representing the official views or policies, either

expressed or implied, of the Defense Advanced Research Projects Agency or the Department of Defense.

NOMENCLATURE

b	mean turbulent fluctuation energy [m^2 s^{-2}]
c_1, c_2	parameters in PSO [-]
c_d	drag resistance coefficient [-]
c_p	specific heat capacity [J kg^{-1} K^{-1}]
D	scale diameter [m]
d_h	porous media hydraulic diameter [m]
∂S_w	internal surface area in the REV [m^2]
e	scale height [m]
f	friction factor [-]
F_p	fin pitch [m]
h	heat transfer coefficient [W m^{-2} K^{-1}]
H	channel height [m]
H_b	base plate thickness [m]
H_f	fin height [m]
k	thermal conductivity [W m^{-1} K^{-1}]

k_T turbulent eddy thermal conductivity [W m^{-1} K^{-1}]

l turbulence mixing length [m]

L_x, L_y, L_z heat sink overall length, width, height [m]

$\langle m \rangle$ local averaged porosity [-]

N_G total number of iterations or generations [-]

N_P total number of individuals in the population; population size [-]

N_S number of individuals in a neighborhood in PSO [-]

p pressure [Pa]

P scale pitch [m]

P_C crossover probability in GA [-]

P_M mutation probability in GA [-]

PP pumping power [W]

R_{th} heat sink thermal resistance, $R_{\text{th}} = \dfrac{\Delta T_{\max}}{\dot{Q}}$, [$^\circ C/W$]

Re $\text{Re} = \dfrac{\tilde{\bar{u}} d_h}{\nu}$ [-]

S_y dimensionless fin pitch, $= F_p / \delta_{\text{base}}$ [-]

S_w local specific surface area $\partial S_w / \Delta\Omega$ [m^{-1}]

T temperature [$^\circ C$]

u	velocity [m s^{-1}]
w	inertia weight in PSO [-]
X	search space vector

Greek

δ	fin thickness [m]
$\Delta T_{\max}$	$\Delta T_{\max} = \tilde{T}_{s,\text{base}}\left(x = L_x, z = -H_b\right) - \tilde{\tilde{T}}_{f,in}$ or $= \tilde{T}_s\left(x = L_x, z = 0\right) - \tilde{\tilde{T}}_{f,in}$ [$°C$]
$\Delta\Omega$	representative elementary volume (REV) [m^3]
μ	dynamic viscosity [kg m^{-1} s^{-1}]
ρ	density [kg m^{-3}]
ν	kinematic viscosity [m^2 s^{-1}]
ν_T	turbulent eddy viscosity [m^2 s^{-1}]

Subscripts and Superscripts

base/top	fin base/top
f	fluid phase
L	laminar
max	maximum
s	solid phase

T	turbulent
x, y, z	x, y, z coordinate directions
~	value in phase averaged over the REV
–	mean turbulent quantity; scaled quantity
′	turbulent fluctuation quantity
*	optimum

REFERENCES

[1] Holland, J. H., 1992, "Adaptation In Natural And Artificial Systems: An Introductory Analysis With Applications To Biology, Control, And Artific."
[2] Goldberg, D. E., 1989, Genetic algorithms in search, optimization, and machine learning, Addison-Wesley Pub. Co., Reading, Mass.
[3] Queipo, N., Devarakonda, R., and Humphrey, J. A. C., 1994, "Genetic algorithms for thermosciences research: application to the optimized cooling of electronic components," International Journal of Heat and Mass Transfer, 37(6), pp. 893-908.
[4] Manivannan, S., Devi, S. P., and Arumugam, R., "Optimization of flat plate heat sink using genetic algorithm," Proc. Electrical Energy Systems (ICEES), 2011 1st International Conference on, pp. 78-81.
[5] Mohsin, S., Maqbool, A., and Khan, W. A., 2009, "Optimization of cylindrical pin-fin heat sinks using genetic algorithms," IEEE Trans. Compon. Packag. Technol. IEEE Transactions on Components and Packaging Technologies, 32(1), pp. 44-52.
[6] Ndao, S., Peles, Y., and Jensen, M. K., 2009, "Multi-objective thermal design optimization and comparative analysis of electronics cooling technologies," International Journal of Heat and Mass Transfer, 52(19-20), pp. 4317-4326.
[7] Fabbri, G., 2000, "Heat transfer optimization in corrugated wall channels," International Journal of Heat and Mass Transfer, 43(23), pp. 4299-4310.
[8] Jian-hui, Z., Chun-xin, Y., and Li-na, Z., 2009, "Minimizing the entropy generation rate of the plate-finned heat sinks using computational fluid dynamics and combined optimization," Applied Thermal Engineering, 29(8-9), pp. 1872-1879.
[9] Wildi-Tremblay, P., and Gosselin, L., 2007, "Layered porous media architecture for maximal cooling," International Journal of Heat and Mass Transfer, 50(3–4), pp. 464-478.
[10] Tye-Gingras, M., and Gosselin, L., 2008, "Thermal Resistance Minimization of a Fin-and-Porous-Medium Heat Sink with Evolutionary Algorithms," Numerical Heat Transfer, Part A: Applications, 54(4), pp. 349-366.

[11] Leblond, G., and Gosselin, L., 2008, "Effect of non-local equilibrium on minimal thermal resistance porous layered systems," International Journal of Heat and Fluid Flow, 29(1), pp. 281-291.
[12] Kennedy, J., and Eberhart, R., "Particle swarm optimization," Proc. Neural Networks, 1995. Proceedings., IEEE International Conference on, pp. 1942-1948 vol.1944.
[13] Eberhart, R., and Kennedy, J., "A new optimizer using particle swarm theory," Proc. Micro Machine and Human Science, 1995. MHS '95., Proceedings of the Sixth International Symposium on, pp. 39-43.
[14] Eberhart, R., and Shi, Y., 1998, "Comparison between genetic algorithms and particle swarm optimization
Evolutionary Programming VII," V. Porto, N. Saravanan, D. Waagen, and A. Eiben, eds., Springer Berlin / Heidelberg, pp. 611-616.
[15] Eberhart, R. C., and Shi, Y., "Comparing inertia weights and constriction factors in particle swarm optimization," Proc. Evolutionary Computation, 2000. Proceedings of the 2000 Congress on, pp. 84-88 vol.81.
[16] Eberhart, and Yuhui, S., "Particle swarm optimization: developments, applications and resources," Proc. Evolutionary Computation, 2001. Proceedings of the 2001 Congress on, pp. 81-86 vol. 81.
[17] Shi, Y., and Eberhart, R. C., "Empirical study of particle swarm optimization," Proc. Evolutionary Computation, 1999. CEC 99. Proceedings of the 1999 Congress on, p. 1950 Vol. 1953.
[18] Xiaohui, H., and Eberhart, R., "Multiobjective optimization using dynamic neighborhood particle swarm optimization," Proc. Evolutionary Computation, 2002. CEC '02. Proceedings of the 2002 Congress on, pp. 1677-1681.
[19] Xiaohui, H., Eberhart, R. C., and Yuhui, S., "Particle swarm with extended memory for multiobjective optimization," Proc. Swarm Intelligence Symposium, 2003. SIS '03. Proceedings of the 2003 IEEE, pp. 193-197.
[20] Bureerat, S., and Srisomporn, S., 2010, "Optimum plate-fin heat sinks by using a multi-objective evolutionary algorithm," Engineering Optimization, 42(4), pp. 305-323.
[21] Kanyakam, S., and Bureerat, S., 2011, "Multiobjective evolutionary optimization of splayed pin-fin heat sink," Engineering Applications of Computational Fluid Mechanics, 5(4), pp. 553-565.
[22] Kanyakam, S., and Bureerat, S., 2012, "Multiobjective Optimization of a Pin-Fin Heat Sink Using Evolutionary Algorithms," Journal of Electronic Packaging, 134(2), pp. 021008-021008.
[23] Catton, I., 2011, "Conjugate Heat Transfer Within a Heterogeneous Hierarchical Structure," Journal of Heat Transfer, 133(10), p. 103001.
[24] Anderson, T. B., and Jackson, R., 1967, "Fluid Mechanical Description of Fluidized Beds. Equations of Motion," Industrial & Engineering Chemistry Fundamentals, 6(4), pp. 527-539.
[25] Slattery, J. C., 1967, "Flow of viscoelastic fluids through porous media," Aiche J, 13(6), pp. 1066-1071.
[26] Marle, C. M., 1967, "Ecoulements monophasiques en milieu poreux," Rev. Inst. Francais du Petrole, 22, pp. 1471-1509.
[27] Whitaker, S., 1967, "Diffusion and dispersion in porous media," AIChE J. AIChE Journal, 13(3), pp. 420-427.

[28] Zolotarev, P. P., and Radushkevich, L. V., 1968, "An approximate analytical solution of the internal diffusion problem of dynamic absorption in the linear region of an isotherm," Russian Chemical Bulletin, 17(8), pp. 1818-1820.
[29] Slattery, J. C., 1980, Momentum, Energy and Mass Transfer in Continua, Krieger, Malabar.
[30] Kaviany, M., 1995, Principles of Heat Transfer in Porous Media, Springer.
[31] Gray, W. G., Leijnse, A., Kolar, R. L., and Blain, C. A., 1993, Mathematical Tools for Changing Spatial Scales in the Analysis of Physical Systems, CRC Press.
[32] Whitaker, S., 1977, "Simultaneous heat, mass and momentum transfer in porous media: a theory of drying," Advances in Heat Transfer, 13, pp. 119-203.
[33] Whitaker, S., 1997, "Volume averaging of transport equations," INTERNATIONAL SERIES ON ADVANCES IN FLUID MECHANICS, 13, pp. 1-60.
[34] Kheifets, L. I., and Neimark, A. V., 1982, "Multiphase Processes in Porous Media," Khimia, Moscow.
[35] Dullien, F. A. L., 1979, Porous Media Fluid Transport and Pore Structure, Academic Press, New York.
[36] Adler, P. M., 1992, Porous Media: Geometry and Transports, Butterworth-Heinemann.
[37] Travkin, V., and Catton, I., 1992, "Models of Turbulent Thermal Diffusivity and Transfer Coefficients for a Regular Packed Bed of Spheres," ASME -PUBLICATIONS- HTD, 193, p. 15.
[38] Travkin, V., and Catton, I., 1995, "A two-temperature model for turbulent flow and heat transfer in a porous layer," Journal of Fluids Engineering, 117(1), pp. 181-188.
[39] Travkin, V. S., and Catton, I., 1998, "Porous media transport descriptions — non-local, linear and non-linear against effective thermal/fluid properties," Advances in Colloid and Interface Science, 76-77(0), pp. 389-443.
[40] Travkin, V. S., Catton, I., and Gratton, L., 1993, "Single Phase Turbulent Transport in Prescribed Non-Isotropic and Stochastic Porous Media," ASME -PUBLICATIONS- HTD, 240, p. 43.
[41] Travkin, V. S., Catton, I., Hu, K., Ponomarenko, A. T., and Shevchenko, V. G., 1999, "Transport Phenomena in Heterogeneous Media: Experimental Data Reduction and Analysis," ASME APPLIED MECHANICS DIVISION -PUBLICATIONS- AMD, 233, pp. 21-32.
[42] Nakayama, A., Ando, K., Yang, C., Sano, Y., Kuwahara, F., and Liu, J., 2009, "A study on interstitial heat transfer in consolidated and unconsolidated porous media," Heat and Mass Transfer, 45(11), pp. 1365-1372.
[43] Nakayama, A., and Kuwahara, F., 2008, "A General Macroscopic Turbulence Model for Flows in Packed Beds, Channels, Pipes, and Rod Bundles," Journal of Fluids Engineering, 130(10), p. 101205.
[44] Nakayama, A., Kuwahara, F., and Hayashi, T., 2004, "Numerical modelling for three-dimensional heat and fluid flow through a bank of cylinders in yaw," Journal of Fluid Mechanics, 498, pp. 139-159.
[45] Nakayama, A., Kuwahara, F., and Kodama, Y., 2006, "An equation for thermal dispersion flux transport and its mathematical modelling for heat and fluid flow in a porous medium," Journal of Fluid Mechanics, 563(1), pp. 81-96.
[46] Travkin, V. S., and Catton, I., 2001, "Transport phenomena in heterogeneous media based on volume averaging theory," Advances in Heat Transfer, G. G. Hari, and A. H. Charles, eds., Elsevier, pp. 1-144.

[47] Geb, D., Zhou, F., deMoulin, G. W., and Catton, I., "Genetic Algorithm Optimization of a Compact Heat Exchanger Modeled Using Volume Averaging Theory," Proc. ASME 2012 Summer Heat Transfer Conference.
[48] Zhou, F., DeMoulin, G. W., Geb, D. J., and Catton, I., 2012, "Closure for a plane fin heat sink with scale-roughened surfaces for volume averaging theory (VAT) based modeling," International Journal of Heat and Mass Transfer, 55(25–26), pp. 7677-7685.
[49] Shi, Y., and Eberhart, R., "A modified particle swarm optimizer," Proc. Evolutionary Computation Proceedings, 1998. IEEE World Congress on Computational Intelligence., The 1998 IEEE International Conference on, pp. 69-73.
[50] Xiaohui, H., Yuhui, S., and Eberhart, R., "Recent advances in particle swarm," Proc. Evolutionary Computation, 2004. CEC2004. Congress on, pp. 90-97 Vol.91.
[51] Holland, J. H., 1992, Adaptation in natural and artificial systems: an introductory analysis with applications to biology, control, and artificial intelligence, MIT press.
[52] Chang, S. W., Liou, T.-M., and Lu, M. H., 2005, "Heat transfer of rectangular narrow channel with two opposite scale-roughened walls," International Journal of Heat and Mass Transfer, 48(19-20), pp. 3921-3931.
[53] Lyons, A., Krishnan, S., Mullins, J., Hodes, M., and Hernon, D., "Advanced heat sinks enabled by three-dimensional printing," Proc. Twentieth Annual International Solid Freeform Fabrication Symposium.
[54] Kays, W. M., and London, A. L., 1984, Compact heat exchangers, McGraw-Hill, New York.

LIST OF FIGURES

LIST OF TABLES

Tables

Parameter	Minimum	Maximum
Fin thickness at base, δ_{base} (mm)	1.50	5.00
Fin thickness at top, δ_{top} (mm)	1.50	5.00
Fin height, H_f (mm)	10.00	23.90
Pitch/fin thickness at base, S_y (-)	1.40	3.00

Table 1: Design parameter ranges for the straight-fin heat sinks

N_P	N_G	N_S	c_1	c_2	w
20	150	5	2.00	2.00	1.00

Table 2: PSO operation settings

N_P	N_G	P_C	P_M
20	300	0.90	0.05

Table 3: GA operation settings

Parameter	Selected Value	
	PSO	**GA**
Fin thickness at base, δ_{base} (mm)	1.50	1.50
Fin thickness at top, δ_{top} (mm)	1.50	1.50
Fin height, H_f (mm)	23.90	23.66
Pitch/fin thickness at base, S_y (-)	1.75	1.75
Thermal Resistance, R_{th}, without base plate (°C/W)	0.079	0.079
Thermal Resistance, R_{th}, with base plate (°C/W)	0.086	0.086

Table 4: Characteristics of optimized smooth surface straight-fin heat sink for PSO and GA methods

Parameter	Selected Value	
	PSO	**GA**
Fin thickness at base, δ_{base} (mm)	1.50	1.50
Fin thickness at top, δ_{top} (mm)	1.50	1.50
Fin height, H_f (mm)	23.90	23.78
Pitch/fin thickness at base, S_y (-)	2.58	2.58
Thermal Resistance, R_{th}, without base plate (°C/W)	0.056	0.056
Thermal Resistance, R_{th}, with base plate (°C/W)	0.058	0.058

Table 5: Characteristics of optimized scale-roughened surface straight-fin heat sinks for PSO and GA methods

	δ_{base}	δ_{top}	H_f	S_y	R_{th} with base
a)	2.43	2.00	16.46	1.67	0.081
b)	2.16	1.50	23.90	1.73	0.068
c)	1.50	1.50	23.90	2.58	0.058
d)	1.50	1.50	23.90	1.75	0.086

Table 6: Characteristics of the heat sinks considered in Figure 8

Figures

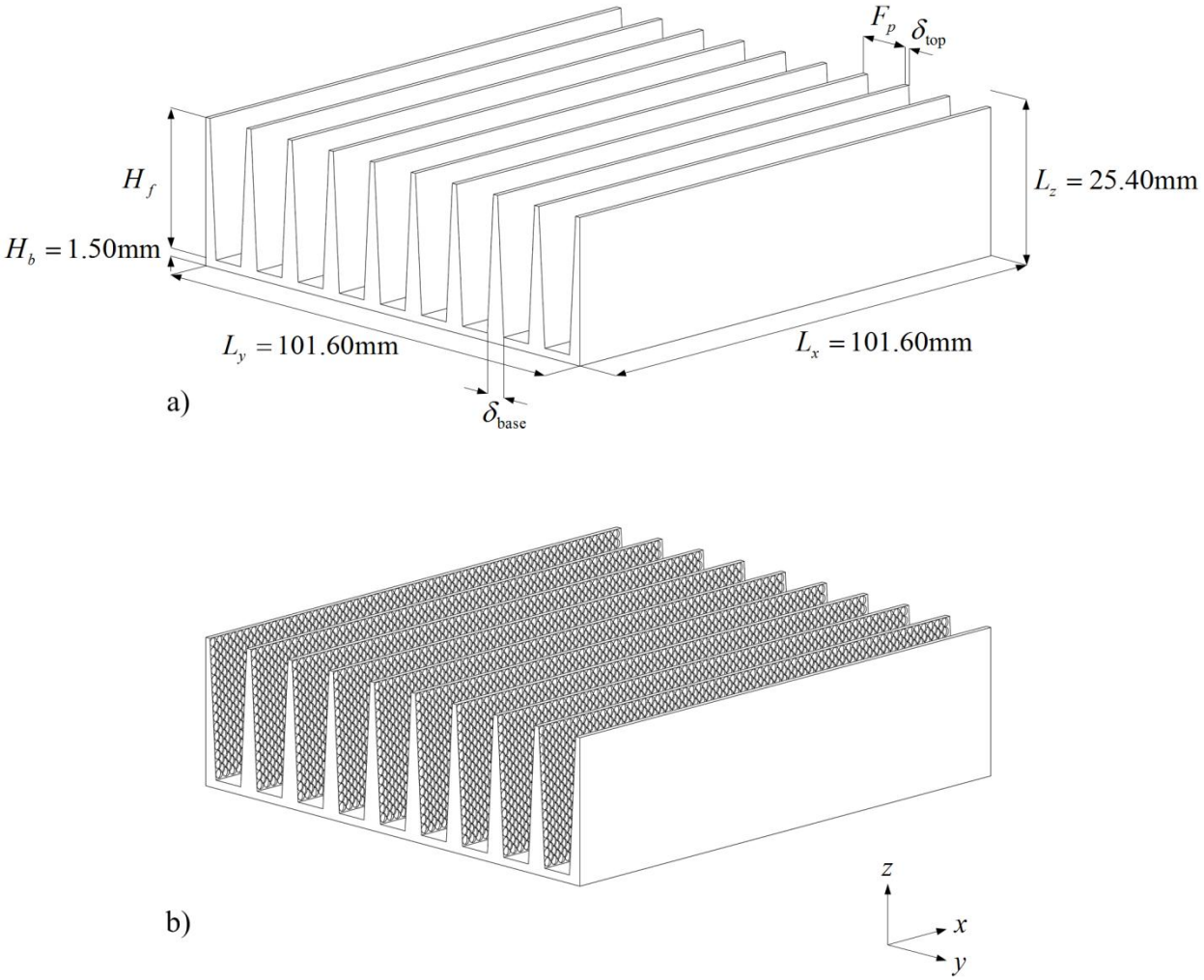

Figure 1: Illustration of a straight-fin heat sink with tapered, a) smooth and b) scale-roughed surface fins

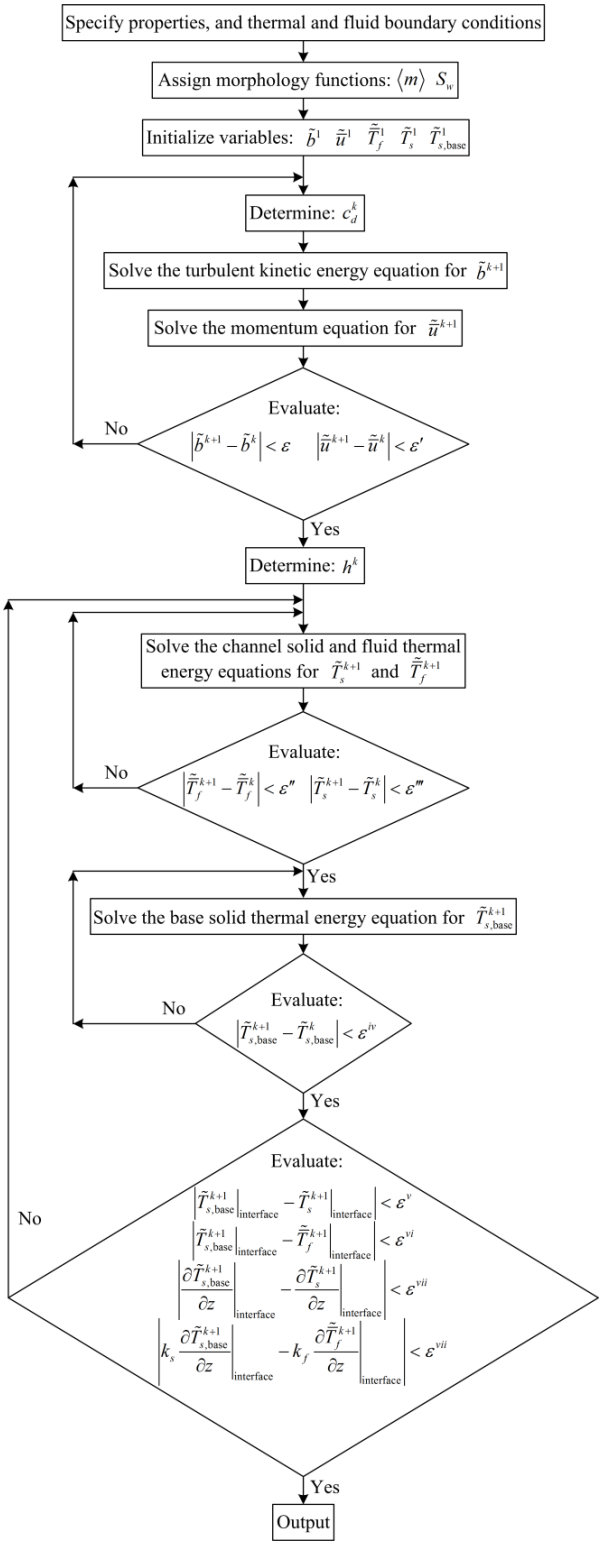

Figure 2: Flow chart of the VAT-based heat sink simulation routine

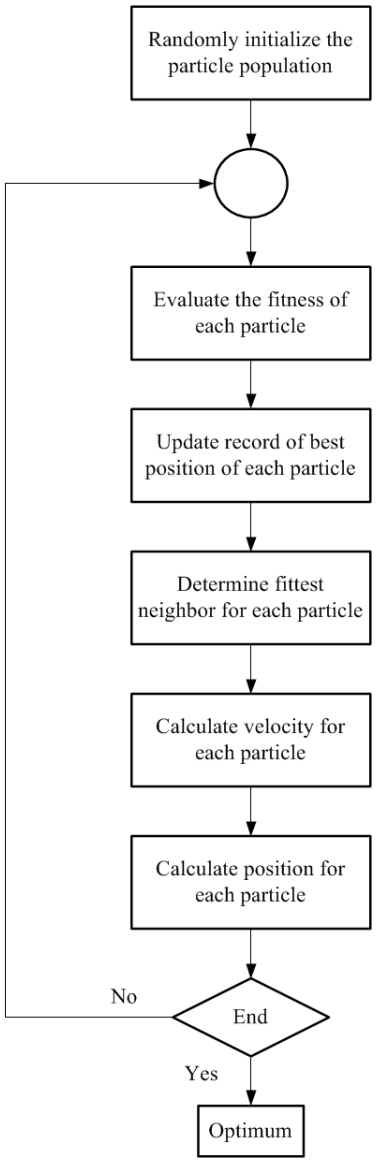

Figure 3: Flow chart of PSO algorithm

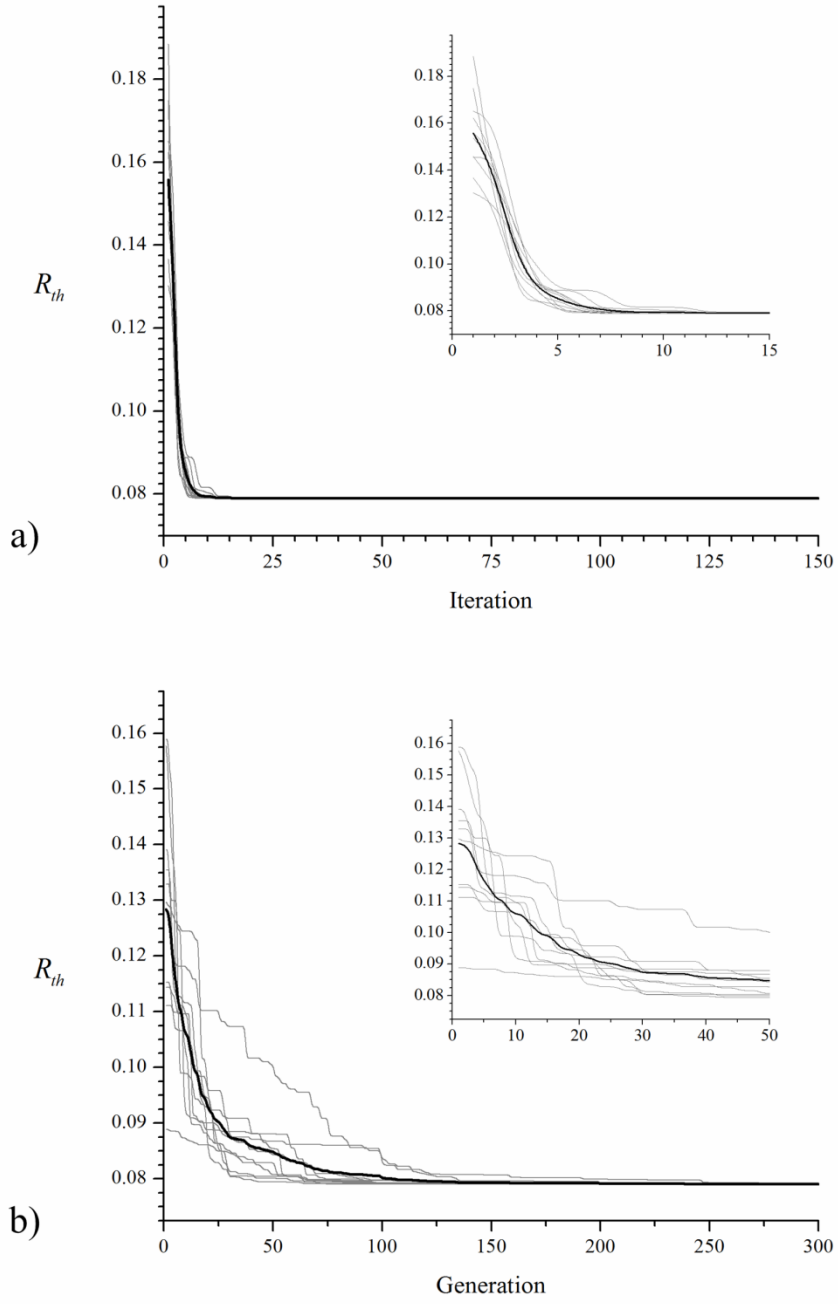

Figure 4: Evolution of thermal resistance during the a) PSO and b) GA optimizations of a smooth surface straight-fin heat sink. Thin, light colored lines indicate the individual trials while thick, dark colored lines indicate the average of the ten trials.

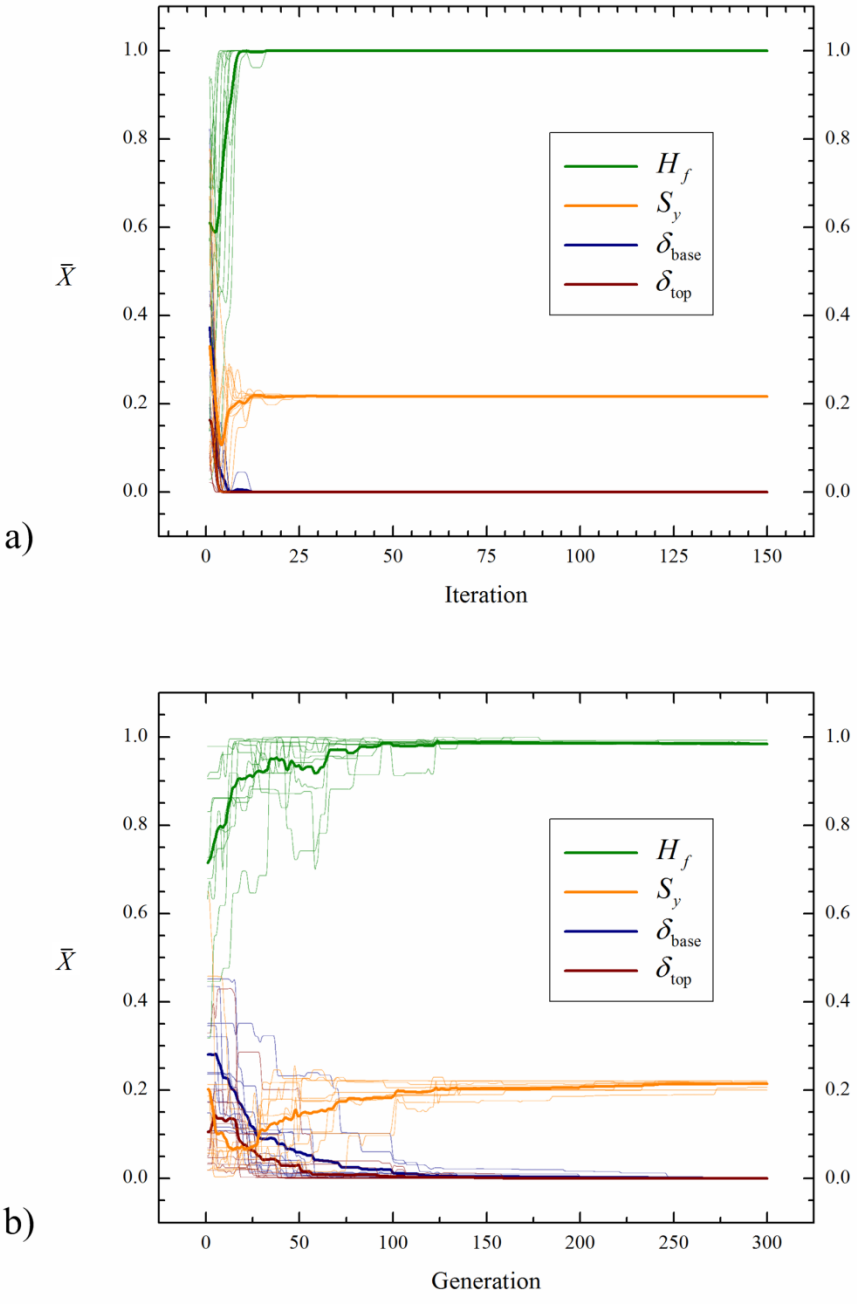

Figure 5: Evolution of the scaled design parameters during the a) PSO and b) GA optimizations of a smooth surface straight-fin heat sink. Thin, light colored lines indicate the individual trials while thick, dark colored lines indicate the average of the ten trials.

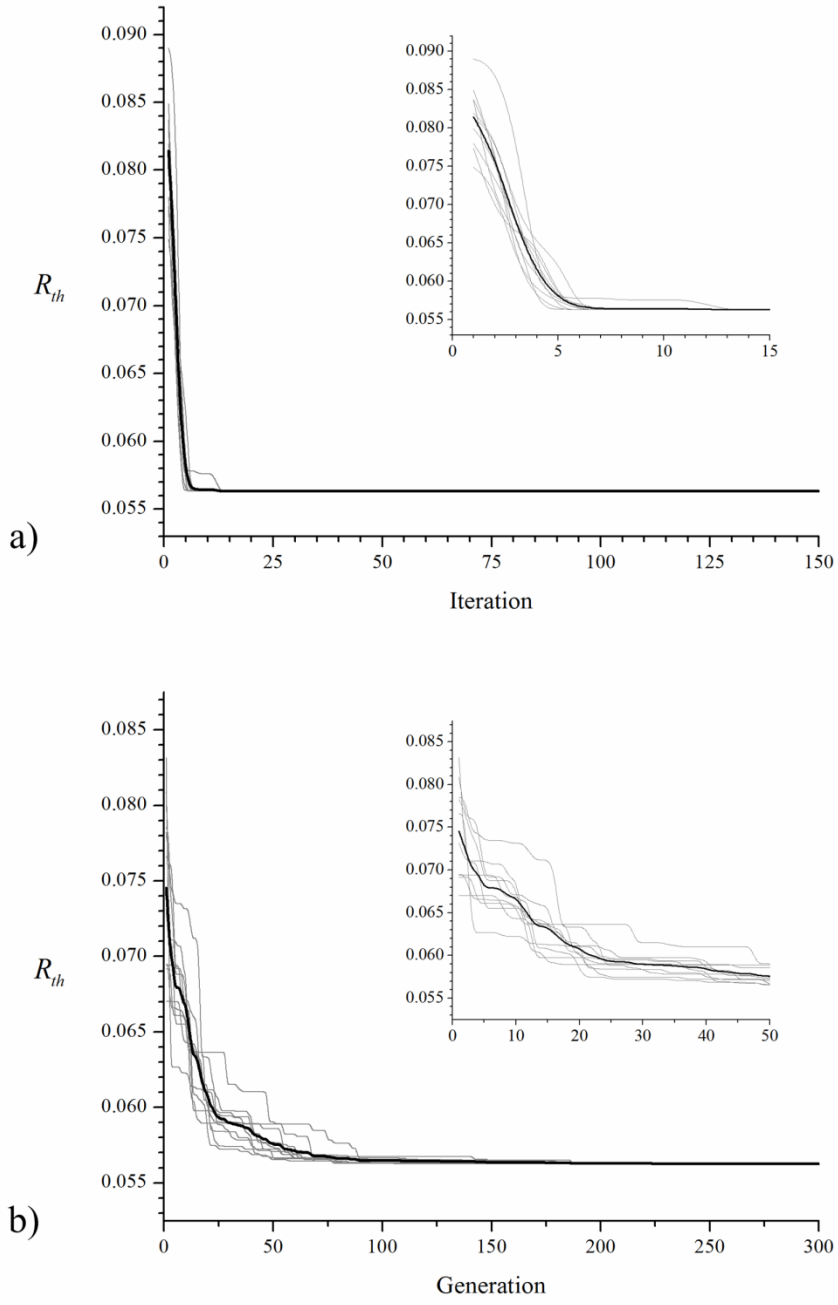

Figure 6: Evolution of thermal resistance during the a) PSO and b) GA optimizations of a scale-roughened straight-fin heat sink

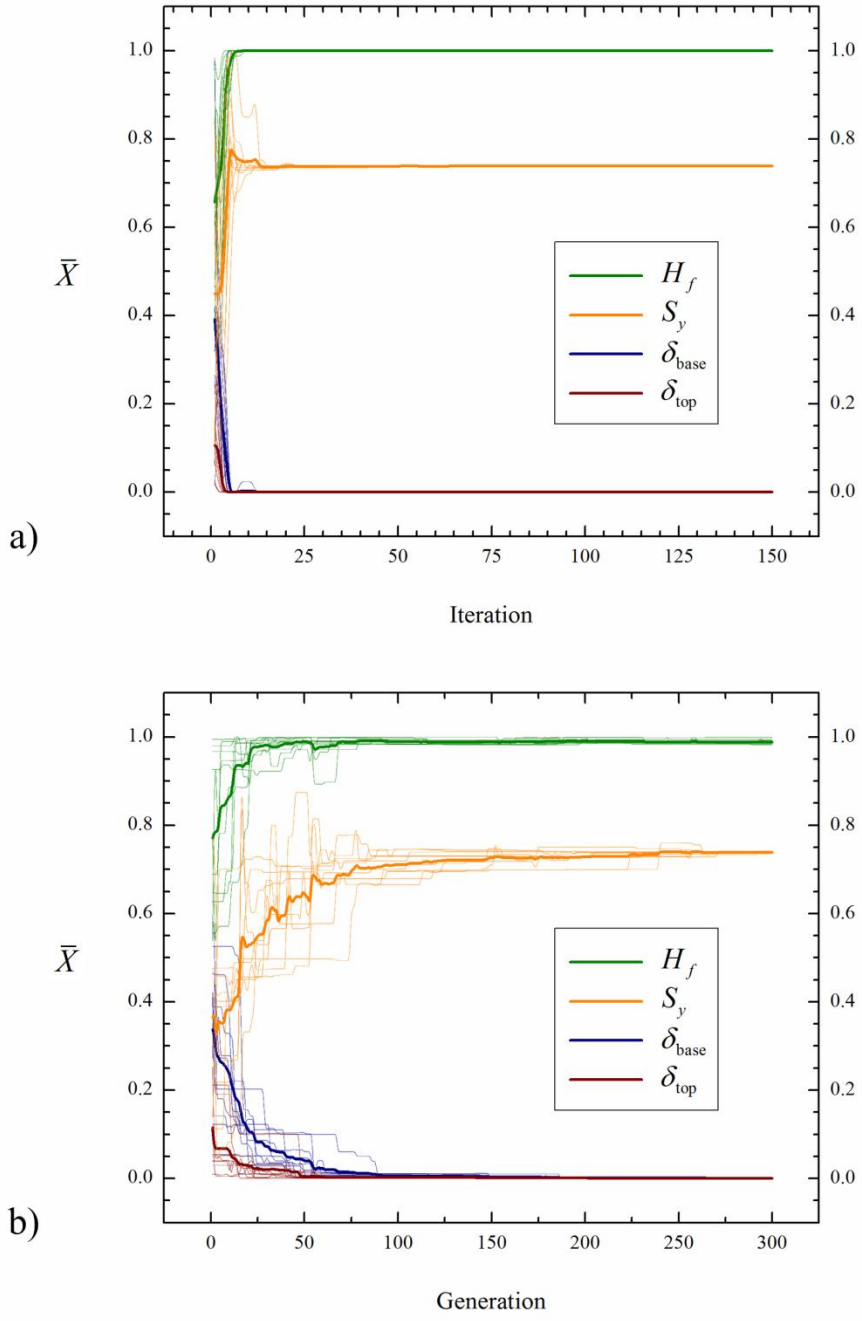

Figure 7: Evolution of the scaled design parameters during the a) PSO and b) GA optimizations of a scale-roughened straight-fin heat sink

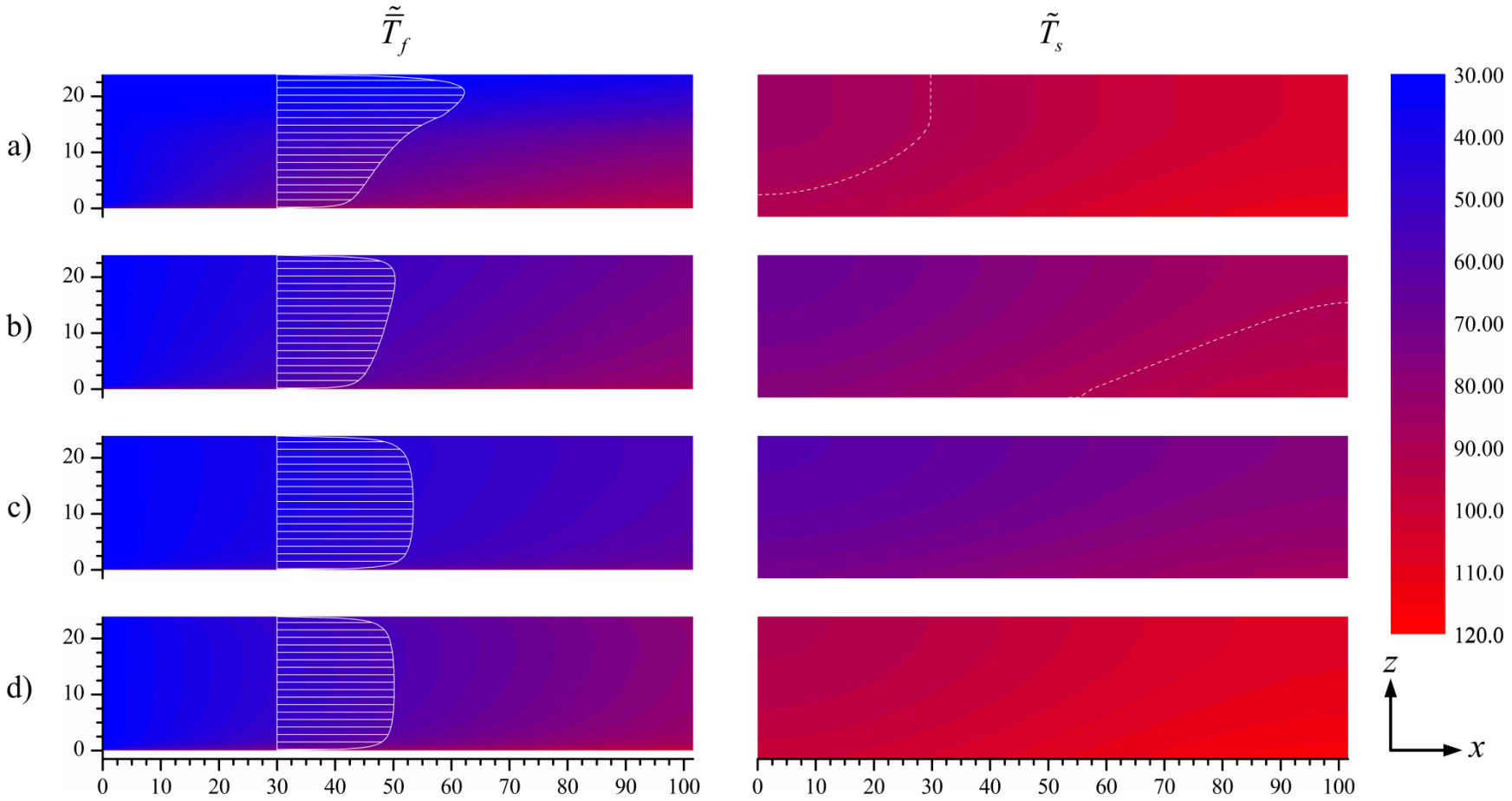

Figure 8: Nonlocal fluid (left) and solid (right) temperature fields for the optimal scale-roughened straight-fin heat sink found by the PSO after its a) first, b) fourth, and c) final iteration, along with those for the d) optimal *smooth* straight-fin heat sink. The fully-developed velocity field profiles and the 90°C contour lines are indicated superimposed on the fluid and solid temperature fields respectively.